NANO LETTERS

pubs.acs.org/NanoLett Letter

e_g Occupancy as a Predictive Descriptor for Spinel Oxide Nanozymes

Quan Wang,[#] Chunyu Li,[#] Xiaoyu Wang,[#] Jun Pu, Shuo Zhang, Like Liang, Lina Chen, Ronghua Liu, Wenbin Zuo, Huigang Zhang, Yanhong Tao, Xingfa Gao, and Hui Wei*

Cite This: *Nano Lett.* 2022, 22, 10003−10009 Read Online

ACCESS | Metrics & More | Article Recommendations | Supporting Information

ABSTRACT: Functional nanomaterials offer an attractive strategy to mimic the catalysis of natural enzymes, which are collectively called nanozymes. Although the development of nanozymes shows a trend of diversification of materials with enzyme-like activity, most nanozymes have been discovered via trial-and-error methods, largely due to the lack of predictive descriptors. To fill this gap, this work identified e_g occupancy as an effective descriptor for spinel oxides with peroxidase-like activity and successfully predicted that the e_g value of spinel oxide nanozymes with the highest activity is close to 0.6. The $LiCo_2O_4$ with the highest activity, which is finally predicted, has achieved more than an order of magnitude improvement in activity. Density functional theory provides a rationale for the reaction path. This work contributes to the rational design of high performance nanozymes by using activity descriptors and provides a methodology to identify other descriptors for nanozymes.

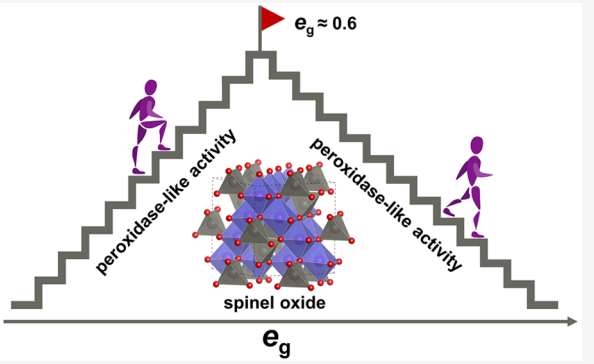

KEYWORDS: *descriptor, rational design, spinel oxide, peroxidase-like, nanozymes*

INTRODUCTION

Nanozymes, defined as nanomaterials with enzyme-like activity, are regarded as emerging alternatives to enzymes because they can overcome intrinsic shortcomings of enzymes (e.g., limited stability under harsh conditions, high cost of preparation, and difficulty in mass production).[1−4] Due to their superior characteristics to conventional enzyme mimics (such as multiple functionalities, large specific surface areas, easy functionalization, and rich and adjustable compositions), nanozymes have shown promising applications in various fields, ranging from nanomedicine to environmental protection and agriculture.[5,6] Over the past decade, a broad spectrum of nanomaterials have been investigated to mimic enzymes, including carbon, metals, metal oxides, metal−organic-frameworks, etc.[7−9]

Despite the considerable progress in the search for various nanomaterials with enzyme-like activity, most of them were discovered by either trial-and-error or serendipity. This is largely due to the lack of guiding principles for rational design of high performance nanozymes. In this respect, while enormous efforts have been invested in the research of peroxidase- (POD-) like nanozymes, only a few studies have revealed key factors governing the activity based on the structure−activity relationship (e.g., Sabatier's rule) (Figure 1a). As a consequence, the activity of the vast majority of POD-like nanozymes is relatively low, which is a gap of several orders of magnitude compared with the activity of natural POD (Figure 1b). Therefore, more effective strategies are needed to design high performance POD-like nanozymes.

Since the report on the POD-like activity of Fe_3O_4 nanoparticles,[10] spinel oxides (AB_2O_4) have attracted great attention due to their well-defined but tunable crystal structures (containing both tetrahedral and octahedral sites at a ratio of 1:2),[11] which is very beneficial for regulating enzyme-like activity[12−17] and discovering predictive descriptors—parameters that indicate enzyme-like activity.[18] Although a variety of descriptors have been reported for other catalysts (especially electrocatalysts),[19−26] the descriptors for nanozymes have rarely been identified, and no descriptors for the enzyme-like activity of spinel oxides have been reported yet.

In this work, we reported for the first time that e_g occupancy is an effective descriptor for the POD-like activity of spinel oxides (e_g stands for the two antibonding molecular orbitals (i.e., $\sigma^*_{x^2-y^2}$ and $\sigma^*_{z^2}$), resulting from the splitting of the d-orbital in an octahedral crystal field), which is not only experimentally measurable but also predictive. We chose ZnB_2O_4 (Zn as a stable tetrahedral site occupancy element) as the model materials[11] and regulated their POD-like activity by adjusting the B site (octahedral site, B = Cr, Mn, Fe, and

Received: September 14, 2022
Revised: December 3, 2022
Published: December 8, 2022

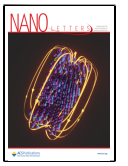

https://doi.org/10.1021/acs.nanolett.2c03598
Nano Lett. 2022, 22, 10003−10009

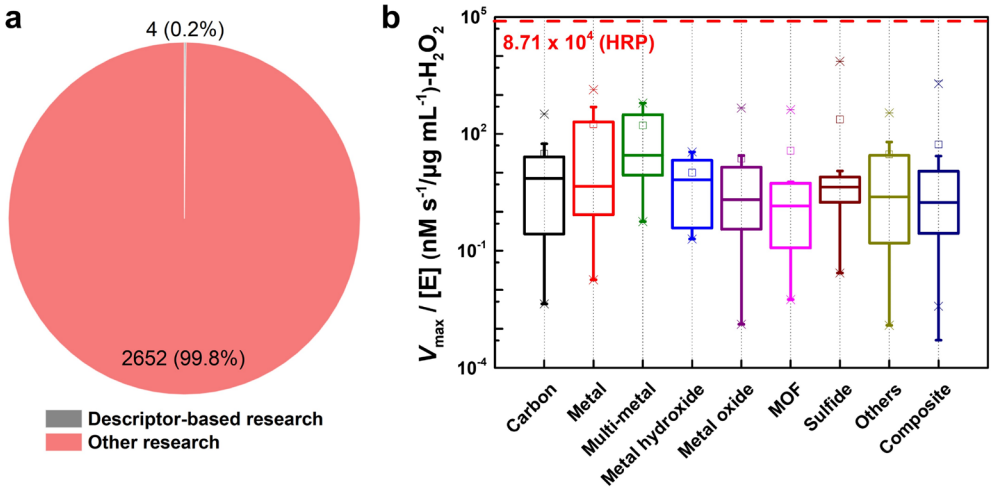

Figure 1. K_{cat} data statistics of different kinds of POD-like nanozymes (the red line is K_{cat} of horseradish peroxidase (HRP)). Here, 2656 articles and 260 data were used, in part from the Supporting Information in ref 5. Statistical classification and data extraction were performed manually.

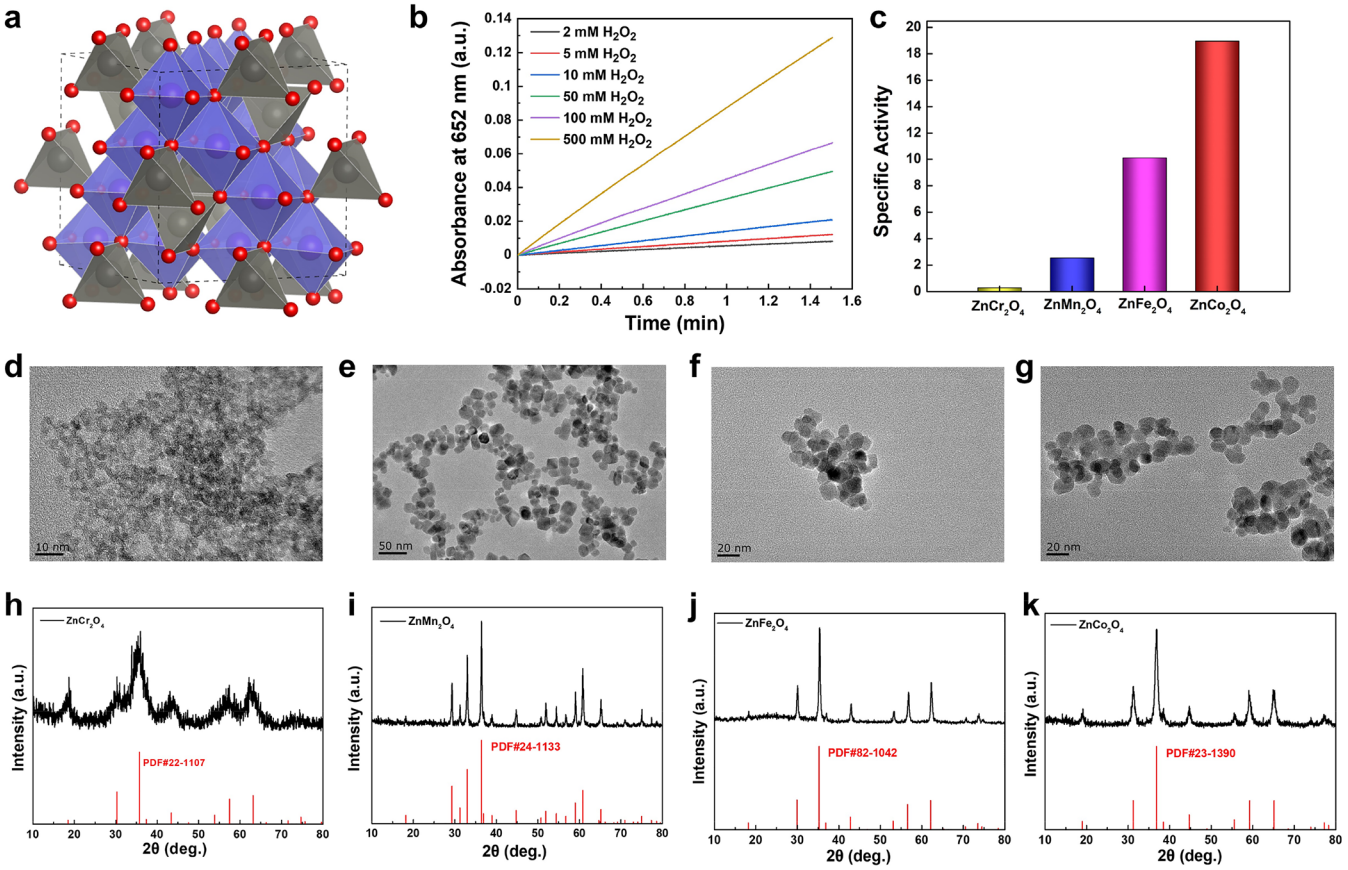

Figure 2. Zn-based spinel oxides as POD mimics. (a) Schematic of ZnB_2O_4 spinel structure, highlighting the octahedral BO_6 structure. Zn, B (transition metal), and O are shown in gray, purple, and red, respectively. (b) Time evolution of absorbance at 652 nm for monitoring the catalytic oxidation of 1 mM TMB with different concentrations of H_2O_2 in the presence of 20 μg/mL $ZnCo_2O_4$. (c) Specific POD-like activities of ZnB_2O_4 (B = Cr, Mn, Fe, and Co). (d–g) TEM images of ZnB_2O_4 (B = Cr, Mn, Fe, and Co). (h–k) XRD patterns of ZnB_2O_4 (B = Cr, Mn, Fe, and Co).

Co) elemental composition. Combining magnetic measurements and other characterizations, we showed that e_g occupancy is a valid descriptor and exhibits a volcano-like curve that predicts the vertices with higher activity. On this basis, we controlled the e_g occupancy of cobalt by doping $ZnCo_2O_4$ with lithium and discovered the material with the highest POD-like activity: $LiCo_2O_4$. Compared with the active parent $ZnCo_2O_4$ in the ZnB_2O_4 system, the activity of predicted $LiCo_2O_4$ was improved by more than an order of magnitude, validating the predictive power of e_g occupancy as a descriptor.

RESULTS AND DISCUSSION

POD-Like Activity of Zn-Based Spinel Oxides. To control the consistency of the crystal structure so that we can

https://doi.org/10.1021/acs.nanolett.2c03598
Nano Lett. 2022, 22, 10003−10009

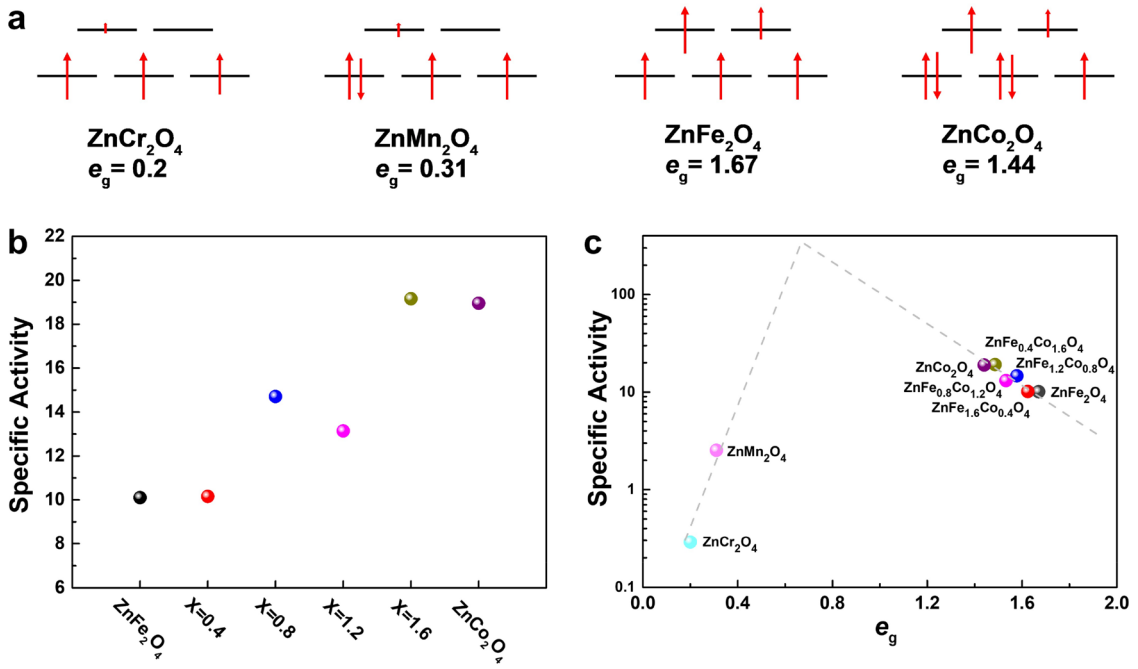

Figure 3. (a) Electron arrangement of d orbitals of ZnB_2O_4 (B = Cr, Mn, Fe, and Co). (b) Specific POD-like activities of $ZnFe_{2-x}Co_xO_4$. (c) Specific POD-like activity of the Zn-based spinel oxides as a function of e_g.

easily find the key factors affecting the activity, we synthesized four zinc-based spinel oxides (ZnB_2O_4, B = Cr, Mn, Fe, and Co) to investigate the effect of the BO_6 octahedral structure on POD-like spinel oxides (Figure 2a). $ZnCr_2O_4$ and $ZnMn_2O_4$ were prepared by a hydrothermal method.[27,28] $ZnFe_2O_4$ and $ZnCo_2O_4$ were prepared by a sol−gel method and annealed at the desired temperatures.[21] The as-prepared spinel oxides were characterized by transmission electron microscopy (TEM) (Figure 2d−g) and powder X-ray diffraction (PXRD) (Figure 2h−k). All samples were uniformly small particles with no specific morphology (less than 25 nm). Their XRD patterns also matched standard cards (red line). These results demonstrated the successful preparation of the materials.

The POD-like activity of zinc-based spinel oxide nanozymes was determined by catalyzing the oxidation of 3,3′,5,5′-tetramethylbenzidine (TMB) with hydrogen peroxide (H_2O_2) in the presence of nanozymes (Figure 2b). The V_{max} of zinc-based spinel oxide nanozymes as mass activity was calculated by drawing a double reciprocal graph through the Michaelis−Menten equation (please refer to the Experimental Section for details) (Figure S1a−h). To exclude the influence of the difference in surface area of nanozymes, the surface area of zinc-based spinel oxide nanozymes was normalized based on the Brunauer−Emmett−Teller (BET) surface area obtained by nitrogen desorption measurements (Figure S2a−d, Table S1) to obtain their specific activities (Figure 2c). It can be seen that whether it was mass activity or specific activity, the trend of activity of this series of materials was consistent, that was $ZnCo_2O_4$ > $ZnFe_2O_4$ > $ZnMn_2O_4$ > $ZnCr_2O_4$. Specifically, the activity of $ZnCo_2O_4$ was about seven times that of $ZnMn_2O_4$, while $ZnCr_2O_4$ showed very weak POD-like activity. These results implied that the octahedral site in the spinel structure profoundly affects the POD-like activity of the materials.

e_g Occupancy as a Descriptor for Spinel Oxide Nanozymes with Peroxidase-like Activity. The above results suggest that regulating the composition of the octahedral site would be an effective way to regulate the enzyme-like activities of spinel oxides. Therefore, we further searched for nanozymes with higher activity by doping Fe and Co at the octahedral site ($ZnFe_{2-x}Co_xO_4$, x = 0.4, 0.8, 1.2, and 1.6), considering that doping is a facile and efficient solution to change the material composition. Of note, $ZnCr_2O_4$ and $ZnMn_2O_4$ were not considered for regulation because of their negligible activity. TEM images showed that the synthesized $ZnFe_{2-x}Co_xO_4$ were all small-sized nanomaterials with no specific morphology (Figure S4a−d). Presumably, the XRD peak position shifted to high angles as the amount of Co doping increased (Figure S5, note that $ZnFe_2O_4$ and $ZnCo_2O_4$ were included here for comparison). After measuring and normalizing the BET surface area (Figure S6a−d, Table S1), the specific activity was obtained using the same method as described above (Figure S2a−h, Figure 3b). Obviously, the $ZnFe_{2-x}Co_xO_4$ series all possessed good POD-like activity, and the activity showed a trend of increase with increasing Co doping amount.

After having optimized some spinel oxide nanozymes with good POD-like activity, it is crucial to reveal the rule that governs spinel oxides to have POD-like activity, which will promote the discovery of predictive descriptors. Since the tetrahedral site is fixed, it is a transition metal cation in the octahedral site with a BO_6 structure that shall affect the activity. The highest occupied orbital (HOMO) of the transition metal involved in the reaction is the d orbital, so it is reasonable to establish a connection between the d orbital filling of the transition metal cation and the activity. Notably, e_g occupancy as a descriptor has been used for electrocatalysts[20,21] and recently for perovskite oxide nanozymes,[18] which indicates its feasibility for spinel oxide nanozymes.

Magnetic measurements were used to determine the zero-field cooling curve of materials, and the number of lone pairs of electrons was calculated according to the Curie−Weiss law (see the experimental section for calculation details) to obtain the arrangement of d-orbital electrons (Figure S7a−h and S8a−h). It should be noted that the data of $ZnCr_2O_4$,

https://doi.org/10.1021/acs.nanolett.2c03598
Nano Lett. 2022, 22, 10003−10009

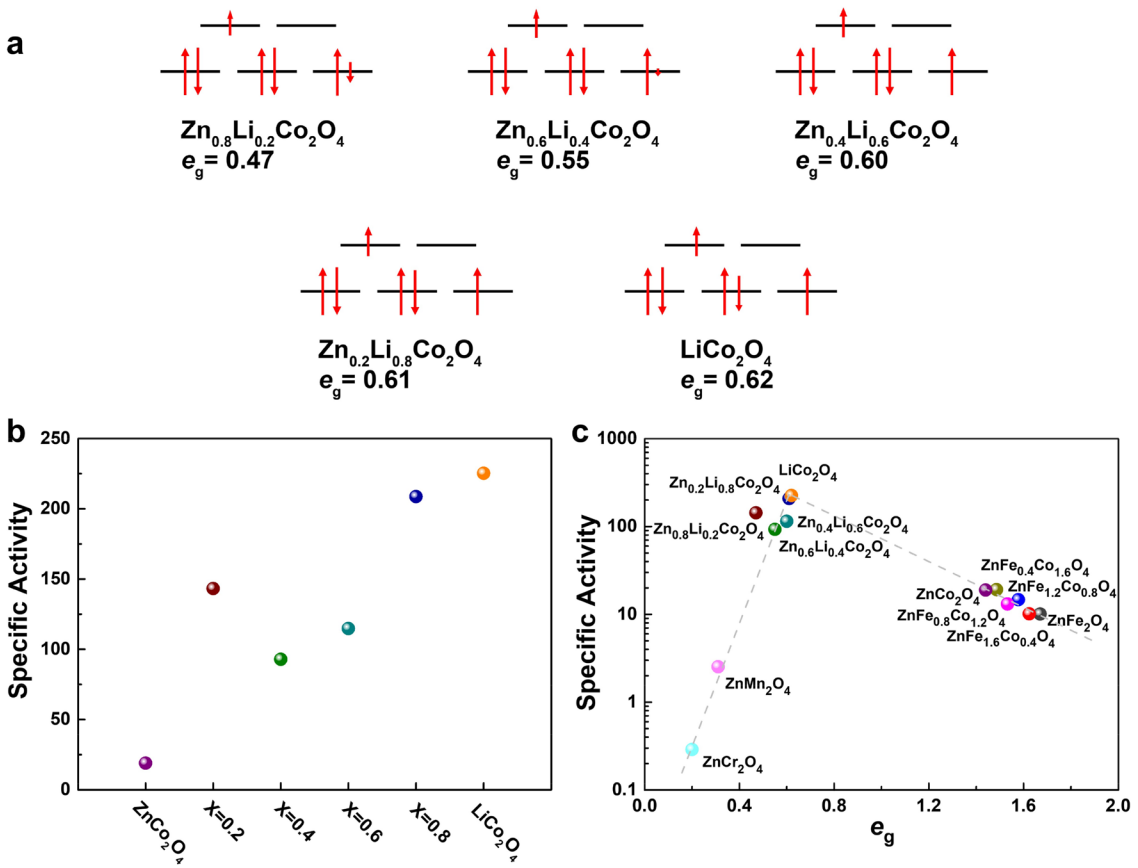

Figure 4. (a) Electron arrangement of d orbitals of $Zn_{1-x}Li_xCo_2O_4$ (x = 0.2, 0.4, 0.6, 0.8, and 1.0). (b) Specific POD-like activities of $Zn_{1-x}Li_xCo_2O_4$. (c) Specific POD-like activity of the spinel oxides as a function of e_g.

$ZnMn_2O_4$, and $ZnCo_2O_4$ had a good linear relationship for calculating μ_{eff} under the test conditions, while the data of $ZnFe_2O_4$ did not satisfy such conditions. Generally, Fe in $ZnFe_2O_4$ is in a high spin state, which was confirmed by Mössbauer spectroscopy (Figure S9a). We used the data of Mössbauer spectroscopy to determine the electron arrangement of Fe. Furthermore, since the vacancy defect of spinel oxide is a cation vacancy,[21] inductively coupled plasma mass spectrometry (ICP−MS) was used to determine the exact chemical formula of a material (Table S2), and this result was used to correct the molar mass and valence state of the metal element at the octahedral site used in the calculation. The $ZnFe_{2-x}Co_xO_4$ (x = 0.4, 0.8, 1.2, and 1.6) series had similar magnetic measurement results to $ZnFe_2O_4$ (Figure S8a−h), and similarly, we used Mössbauer spectroscopy to demonstrate the high spin state of Fe (Figure S9b−e). Since the $ZnFe_{2-x}Co_xO_4$ series samples have two metal elements on the octahedral sites, the e_g value we calculated used the weighted combination of Co and Fe to represent the e_g value of a BO_6 structure.

After the necessary corrections were made to the electron arrangement of the d orbital, the final electron arrangement results were obtained (Figure 3a). Interestingly, when we use e_g occupancy as the x-axis and the specific activity of spinel oxide nanozymes as the y-axis, a strong and nonmonotonic correlation (volcanic curve) appears between e_g occupancy and the POD-like activity of spinel oxides (Figure 3c), suggesting that e_g occupancy as an activity descriptor is suitable for spinel oxide systems. On the left half of the volcanic curve, the occupancies of $ZnCr_2O_4$ and $ZnMn_2O_4$ are 0.2 and 0.31, respectively, and on the right half of the curve, the occupancies of $ZnCo_2O_4$, $ZnFe_{0.4}Co_{1.6}O_4$, $ZnFe_{0.8}Co_{1.2}O_4$, $ZnFe_{1.2}Co_{0.8}O_4$, $ZnFe_{1.6}Co_{0.4}O_4$, and $ZnFe_2O_4$ are 1.44, 1.49, 1.53, 1.58, 1.62 and 1.67, respectively. Encouragingly, it was expected that the materials occupying the apex of the volcanic curve should have a higher activity. Therefore, it was necessary to synthesize these materials with an e_g occupancy between 0.31 and 1.44 and investigate their POD-like activity.

Tuning the e_g Occupancy to Optimize a Spinel Oxide with the Highest Peroxidase-like Activity. Under the prediction of the e_g descriptor, we then adjusted the e_g value of spinel oxide nanozymes by a suitable method to obtain better nanozymes. For the $ZnFe_{2-x}Co_xO_4$ series, $ZnCo_2O_4$ with the lowest e_g value has the highest activity (Figure 3c). Therefore, it was reasonable to further lower the e_g value of Co (i.e., increase the valence of Co) to improve the POD-like activity with an appropriate method (such as introducing stable monovalent lithium at the tetrahedral site). Therefore, we synthesized $Zn_{1-x}Li_xCo_2O_4$ (x = 0.2, 0.4, 0.6, 0.8, and 1.0), and these materials had a small size (~20 nm) and no special morphology, similar to the above materials (Figure S10a−e). With the increase in the amount of Li incorporated, the XRD peak position shifted to high angles (Figure S11). The lone pair electrons of $Zn_{1-x}Li_xCo_2O_4$ were measured by magnetic measurement, and the e_g values were calculated (Figure S14a−j). After the molecular weight and valence state of metal elements were corrected by ICP−AES (Table S2), as expected, the strategy of regulating the e_g value was effective, and the e_g occupancy of the synthesized $Zn_{1-x}Li_xCo_2O_4$ series materials

https://doi.org/10.1021/acs.nanolett.2c03598
Nano Lett. 2022, 22, 10003−10009

were all smaller than 1.44 (the e_g value of $ZnCo_2O_4$) (Figure 4a).

As shown in Figure 4b, the specific activity was obtained after BET surface area normalization (Figure S12a−e, Figure S13a−j, and Table S1). We were surprised to find that the activity of $Zn_{1-x}Li_xCo_2O_4$ continues to increase with increasing lithium doping, and this increase in activity is very large. This may indicate the predictive power of e_g as a descriptor. The e_g values and μ_{eff} for all materials are listed in Table S3. Based on this, we supplemented the e_g value and specific activity data of $Zn_{1-x}Li_xCo_2O_4$ and plotted Figure 4c. We can see that the newly measured data not only confirm the trend of the volcanic curve but also reveal that $LiCo_2O_4$ happens to occupy the apex of the volcanic curve as a spinel oxide material with the highest POD-like activity. Moreover, it is worth noting that compared with $ZnCo_2O_4$ with the best POD-like activity in the ZnB_2O_4 series, the predicted $LiCo_2O_4$ still has an order of magnitude advantage. All these results confirm the applicability of e_g as a descriptor of spinel oxide with POD-like activity and prove the predictive and guiding significance of e_g as a descriptor of this system.

For the prediction of the best material obtained, $LiCo_2O_4$, we also performed a systematic stability study. There was only a slight decrease in the activity of $LiCo_2O_4$ after 1 year (Figure S15), which demonstrates the long-term stability and ease of preservation. In addition, the results of cycling experiments (Figure S16) and XRD characterization (Figure S17) of $LiCo_2O_4$ after the reaction further confirmed the stability of the material. The temperature and pH-dependent behavior of $LiCo_2O_4$ were also tested (Figure S18). The results showed that $LiCo_2O_4$ exhibited significant activity in acidic environments, and the activity gradually increased with increasing temperature. To clearly demonstrate the advantages of the predicted obtained materials in terms of activity, we listed some typical metal oxide nanozymes with peroxidase-like activity for comparison with $LiCo_2O_4$ (Table S4).

DFT Calculations. DFT calculations were performed to explore the structure−activity relationship for the POD-like activities of the synthesized spinel oxides and to reveal the underlying reason for their relative activity order. The (440) facets of $LiCo_2O_4$, $ZnCo_2O_4$, $ZnFe_2O_4$, $ZnMn_2O_4$, and $ZnCr_2O_4$ were considered as the active surfaces in accordance with the experiment. Unlike the bulk B atoms, which are six-coordinated, surface B atoms have unsaturated four-coordinated conformations and thus are considered as the active centers. A possible mechanism is proposed to explain the POD-like activities of spinel oxides: (i) the dissociative chemisorption of H_2O_2 on the surfaces generating the dihydroxyl intermediates; (ii and iii) two successive processes in which the adsorbed hydroxyls abstract H atoms form the TMB substrate and leave from the catalyst surface in the form of H_2O (Figure 5a).

The structures of intermediates involved in the catalysis are shown in Figure S19b. According to the energy profiles in Figure 5b, reaction steps i of all five surfaces are highly exothermic, with reaction energies (E_r) ranging from −2.57 for $ZnCo_2O_4$ to −5.23 eV for $ZnCr_2O_4$. In addition, the calculations could not locate physisorption configurations for H_2O_2 on these surfaces, suggesting that H_2O_2 molecules should quickly dissociate into hydroxyl adsorbates when approaching the surfaces. The facile dissociation of H_2O_2 indicates that step i is not the rate-determining step (RDS) for the catalysis. In contrast, steps ii and iii are all endothermic.

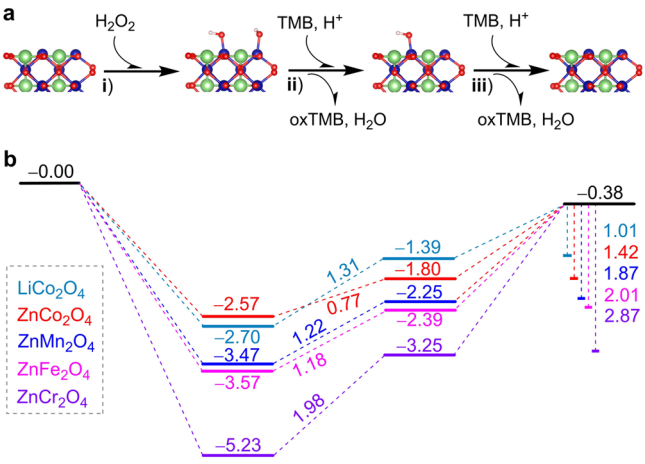

Figure 5. DFT calculation results. (a) Mechanism proposed for the POD-like catalysis of spinels. (b) Energy profiles in eV corresponding to the proposed mechanism. The relative energies (eV) for each stationary point involved in the catalytic cycles and the reaction energy for each reaction step of hydroxyl removal are labeled.

Step iii is more endothermic than the corresponding step ii for all the surfaces except for $LiCo_2O_4$. These reaction steps are described with the following equations:

$$H_2O_2 + 2^* = 2OH^* \quad \text{(i)}$$

$$OH^{1*} + TMB + H^+ = H_2O + oxTMB \quad \text{(ii)}$$

$$OH^{2*} + TMB + H^+ = H_2O + oxTMB \quad \text{(iii)}$$

In the above equations, surface adsorption sites are designated by asterisks; species labeled with an asterisk mean surface adsorbates; and OH^{1*} and OH^{2*} represent the two hydroxyl adsorbates. Therefore, step (ii) is the RDS for $LiCo_2O_4$, and step (iii) is the RDS for the remaining four surfaces. The E_r of the RDS increases in this order: 1.39 eV ($LiCo_2O_4$) < 1.42 eV ($ZnCo_2O_4$) < 1.87 eV ($ZnMn_2O_4$) < 2.01 eV ($ZnFe_2O_4$) < 2.87 eV ($ZnCr_2O_4$). A lower E_r means that the hydroxyl adsorbate is thermodynamically easier to remove from the surface, corresponding to a higher POD-like activity. Therefore, the activity should decrease in the order $LiCo_2O_4$ > $ZnCo_2O_4$ > $ZnMn_2O_4$ > $ZnFe_2O_4$ > $ZnCr_2O_4$, which is in general agreement with the experimental observations except for the activity order of $ZnFe_2O_4$ and $ZnMn_2O_4$. This inconsistency may be due to the current limitations of computation and modeling. It is inferred that the e_g occupancy influences the d-band energies of the materials surfaces and consequently the adsorption affinity of the surfaces for OH*.[29] This may be the reason that the e_g occupancy influences the catalytic activity of the surfaces. The atomistic-level mechanism for the e_g dependent activity deserves further investigation in the future.

CONCLUSION

By exploring a series of spine oxides, we found the key factor affecting their POD-like activity—e_g occupancy. The e_g occupancy as a descriptor predicts that the spinel oxide with the highest POD-like activity will appear when e_g is near 0.6. Encouragingly, for a series of materials ($Zn_{1-x}Li_xCo_2O_4$) with an e_g value around 0.6, we showed that their POD-like activity was in line with the volcanic curve. Among these materials, $LiCo_2O_4$ with an e_g = 0.62 has the highest activity and has

https://doi.org/10.1021/acs.nanolett.2c03598
Nano Lett. 2022, 22, 10003−10009

more than an order of magnitude improvement, which reflects the predictive power and high efficiency of e_g occupancy as a descriptor of spinel oxides with POD-like activity. DFT calculations thoroughly investigate the catalysis process and provide a detailed mechanistic explanation of the reaction path. As the first descriptor reported in the spinel oxide system, the predictive power of e_g descriptors is fully demonstrated, which will greatly promote research on the activity and application of spinel oxide nanozymes as well as inspire us and others to identify other descriptors for nanozymes.

■ ASSOCIATED CONTENT

Supporting Information

The Supporting Information is available free of charge at https://pubs.acs.org/doi/10.1021/acs.nanolett.2c03598.

Experimental section, kinetic data, ICP, BET areas, XRD and TEM images, magnetic data, Mössbauer spectra, μ_{eff} and corrected e_g values, stability of $LiCo_2O_4$, pH and temperature-dependent activity of $LiCo_2O_4$, geometrically optimized structures, and crystallographic data (PDF)

■ AUTHOR INFORMATION

Corresponding Author

Hui Wei − *College of Engineering and Applied Sciences, Nanjing National Laboratory of Microstructures, Jiangsu Key Laboratory of Artificial Functional Materials and State Key Laboratory of Analytical Chemistry for Life Science, School of Chemistry and Chemical Engineering, Chemistry and Biomedicine Innovation Center (ChemBIC), Nanjing University, Nanjing, Jiangsu 210023, China;* orcid.org/0000-0003-0870-7142; Email: weihui@nju.edu.cn

Authors

Quan Wang − *College of Engineering and Applied Sciences, Nanjing National Laboratory of Microstructures, Jiangsu Key Laboratory of Artificial Functional Materials, Nanjing University, Nanjing, Jiangsu 210023, China*

Chunyu Li − *College of Chemistry and Chemical Engineering, Jiangxi Normal University, Nanchang, Jiangxi 330022, China*

Xiaoyu Wang − *College of Engineering and Applied Sciences, Nanjing National Laboratory of Microstructures, Jiangsu Key Laboratory of Artificial Functional Materials, Nanjing University, Nanjing, Jiangsu 210023, China; Department of Chemistry and Material Science, College of Science, Nanjing Forestry University, Nanjing, Jiangsu 210037, China;* orcid.org/0000-0002-8641-2430

Jun Pu − *Key Laboratory of Functional Molecular Solids, Ministry of Education, College of Chemistry and Materials Science, Anhui Normal University, Wuhu, Anhui 241002, China;* orcid.org/0000-0001-9393-3798

Shuo Zhang − *College of Engineering and Applied Sciences, Nanjing National Laboratory of Microstructures, Jiangsu Key Laboratory of Artificial Functional Materials, Nanjing University, Nanjing, Jiangsu 210023, China*

Like Liang − *Jiangsu Provincial Key Laboratory for Nanotechnology, National Laboratory of Solid State Microstructures and School of Physics, Nanjing University, Nanjing, Jiangsu 210023, China*

Lina Chen − *School of Science, Nanjing University of Posts and Telecommunications, Nanjing, Jiangsu 210023, China*

Ronghua Liu − *Jiangsu Provincial Key Laboratory for Nanotechnology, National Laboratory of Solid State Microstructures and School of Physics, Nanjing University, Nanjing, Jiangsu 210023, China;* orcid.org/0000-0002-4053-3923

Wenbin Zuo − *School of Physics and Technology, Wuhan University, Wuhan, Hubei 430072, China*

Huigang Zhang − *College of Engineering and Applied Sciences, Nanjing National Laboratory of Microstructures, Jiangsu Key Laboratory of Artificial Functional Materials, Nanjing University, Nanjing, Jiangsu 210023, China;* orcid.org/0000-0002-4722-5384

Yanhong Tao − *College of Chemistry and Chemical Engineering, Jiangxi Normal University, Nanchang, Jiangxi 330022, China*

Xingfa Gao − *College of Chemistry and Chemical Engineering, Jiangxi Normal University, Nanchang, Jiangxi 330022, China; Laboratory of Theoretical and Computational Nanoscience, National Center for Nanoscience and Technology of China, Beijing 100190, China;* orcid.org/0000-0002-1636-6336

Complete contact information is available at: https://pubs.acs.org/10.1021/acs.nanolett.2c03598

Author Contributions

#Q.W., C.L., and X.W. contributed equally to this paper.

Notes

The authors declare no competing financial interest.

■ ACKNOWLEDGMENTS

We thank Prof. Yueming Zhai for his help with Mössbauer spectra measurements, Prof. You Song and Liya Lv for their help and advice on magnetic measurements and calculations, and Prof. Ying-Wu Lin for his discussion. Funding: This work was supported by the National Key R&D Program of China (2019YFA0709200 and 2021YFF1200700), Jiangsu Provincial Key R&D Program (BE2022836), National Natural Science Foundation of China (22104055, 21874067, and 21722503), the Innovation Foundation of Nanjing University, PAPD Program, Fundamental Research Funds for the Central Universities (202200325 and 021314380195), and Interdisciplinary Project Funded by Graduate School of Nanjing University (2018CL13).

■ REFERENCES

(1) Wei, H.; Wang, E. Nanomaterials with enzyme-like characteristics (nanozymes): next-generation artificial enzymes. *Chem. Soc. Rev.* **2013**, *42* (14), 6060−6093.

(2) Zhang, X.; Huang, R.; Gopalakrishnan, S.; Cao-Milán, R.; Rotello, V. M. Bioorthogonal nanozymes: progress towards therapeutic applications. *Trends Chem.* **2019**, *1* (1), 90−98.

(3) Liang, M.; Yan, X. Nanozymes: from new concepts, mechanisms, and standards to applications. *Acc. Chem. Res.* **2019**, *52* (8), 2190−2200.

(4) Huang, Y.; Ren, J.; Qu, X. Nanozymes: classification, catalytic mechanisms, activity regulation, and applications. *Chem. Rev.* **2019**, *119* (6), 4357−4412.

(5) Wu, J.; Wang, X.; Wang, Q.; Lou, Z.; Li, S.; Zhu, Y.; Qin, L.; Wei, H. Nanomaterials with enzyme-like characteristics (nanozymes): next-generation artificial enzymes (II). *Chem. Soc. Rev.* **2019**, *48* (4), 1004−1076.

(6) Wei, H.; Gao, L.; Fan, K.; Liu, J.; He, J.; Qu, X.; Dong, S.; Wang, E.; Yan, X. Nanozymes: a clear definition with fuzzy edges. *Nano Today* **2021**, *40*, 101269.

(7) Zhang, R.; Yan, X.; Fan, K. Nanozymes inspired by natural enzymes. *Acc. Mater. Res.* **2021**, *2* (7), 534−547.
(8) Zandieh, M.; Liu, J. Nanozyme catalytic turnover and self-limited reactions. *ACS Nano* **2021**, *15* (10), 15645−15655.
(9) Serrano-Aroca, A.; Takayama, K.; Tunon-Molina, A.; Seyran, M.; Hassan, S. S.; Pal Choudhury, P.; Uversky, V. N.; Lundstrom, K.; Adadi, P.; Palu, G.; Aljabali, A. A. A.; Chauhan, G.; Kandimalla, R.; Tambuwala, M. M.; Lal, A.; Abd El-Aziz, T. M.; Sherchan, S.; Barh, D.; Redwan, E. M.; Bazan, N. G.; Mishra, Y. K.; Uhal, B. D.; Brufsky, A. Carbon-based nanomaterials: promising antiviral agents to combat COVID-19 in the microbial-resistant era. *ACS Nano* **2021**, *15* (5), 8069−8086.
(10) Gao, L.; Zhuang, J.; Nie, L.; Zhang, J.; Zhang, Y.; Gu, N.; Wang, T.; Feng, J.; Yang, D.; Perrett, S.; Yan, X. Intrinsic peroxidase-like activity of ferromagnetic nanoparticles. *Nat. Nanotechnol.* **2007**, *2* (9), 577−583.
(11) Zhao, Q.; Yan, Z.; Chen, C.; Chen, J. Spinels: controlled preparation, oxygen reduction/evolution reaction application, and beyond. *Chem. Rev.* **2017**, *117* (15), 10121−10211.
(12) Zhang, X.; Min, Y.; Zhang, Q.; Wu, S.; Fu, W.; Wu, J.; Li, M.; Wang, Y.; Zhang, P. Functionalized Mn_3O_4 nanosheets with photothermal, photodynamic, and oxidase-like activities triggered by low-powered near-infrared light for synergetic combating multidrug-resistant bacterial infections. *Adv. Healthc. Mater.* **2022**, *11* (12), 2200121.
(13) Cheng, Y.; Cheng, C.; Yao, J.; Yu, Y.; Liu, Y.; Zhang, H.; Miao, L.; Wei, H. Mn_3O_4 nanozyme for inflammatory bowel disease therapy. *Adv. Ther.* **2021**, *4* (9), 2100081.
(14) Yao, J.; Cheng, Y.; Zhou, M.; Zhao, S.; Lin, S.; Wang, X.; Wu, J.; Li, S.; Wei, H. ROS scavenging Mn_3O_4 nanozymes for *in vivo* anti-inflammation. *Chem. Sci.* **2018**, *9* (11), 2927−2933.
(15) Singh, N.; Savanur, M. A.; Srivastava, S.; D'Silva, P.; Mugesh, G. A redox modulatory Mn_3O_4 nanozyme with multi-enzyme activity provides efficient cytoprotection to human cells in a parkinson's disease model. *Angew. Chem., Int. Ed.* **2017**, *56* (45), 14267−14271.
(16) Vernekar, A. A.; Das, T.; Ghosh, S.; Mugesh, G. A remarkably efficient $MnFe_2O_4$-based oxidase nanozyme. *Chem. Asian J.* **2016**, *11* (1), 72−76.
(17) Wang, Q.; Cheng, C.; Zhao, S.; Liu, Q.; Zhang, Y.; Liu, W.; Zhao, X.; Zhang, H.; Pu, J.; Zhang, S.; Zhang, H.; Du, Y.; Wei, H. A valence-engineered self-cascading antioxidant nanozyme for the therapy of inflammatory bowel disease. *Angew. Chem., Int. Ed.* **2022**, *61* (27), e202201101.
(18) Wang, X.; Gao, X. J.; Qin, L.; Wang, C.; Song, L.; Zhou, Y. N.; Zhu, G.; Cao, W.; Lin, S.; Zhou, L.; Wang, K.; Zhang, H.; Jin, Z.; Wang, P.; Gao, X.; Wei, H. e_g occupancy as an effective descriptor for the catalytic activity of perovskite oxide-based peroxidase mimics. *Nat. Commun.* **2019**, *10* (1), 704.
(19) Ren, C.; Lu, S.; Wu, Y.; Ouyang, Y.; Zhang, Y.; Li, Q.; Ling, C.; Wang, J. A universal descriptor for complicated interfacial effects on electrochemical reduction reactions. *J. Am. Chem. Soc.* **2022**, *144* (28), 12874−12883.
(20) Wei, C.; Feng, Z.; Scherer, G. G.; Barber, J.; Shao-Horn, Y.; Xu, Z. J. Cations in octahedral sites: a descriptor for oxygen electrocatalysis on transition-metal spinels. *Adv. Mater.* **2017**, *29* (23), 1606800.
(21) Zhou, Y.; Sun, S.; Song, J.; Xi, S.; Chen, B.; Du, Y.; Fisher, A. C.; Cheng, F.; Wang, X.; Zhang, H.; Xu, Z. J. Enlarged Co-O covalency in octahedral sites leading to highly efficient spinel oxides for oxygen evolution reaction. *Adv. Mater.* **2018**, *30* (32), 1802912.
(22) Tao, H. B.; Fang, L.; Chen, J.; Yang, H. B.; Gao, J.; Miao, J.; Chen, S.; Liu, B. Identification of surface reactivity descriptor for transition metal oxides in oxygen evolution reaction. *J. Am. Chem. Soc.* **2016**, *138* (31), 9978−85.
(23) Jacobs, R.; Hwang, J.; Shao-Horn, Y.; Morgan, D. Assessing correlations of perovskite catalytic performance with electronic structure descriptors. *Chem. Mater.* **2019**, *31* (3), 785−797.
(24) Guo, C.; Tian, X.; Fu, X.; Qin, G.; Long, J.; Li, H.; Jing, H.; Zhou, Y.; Xiao, J. Computational design of spinel oxides through coverage-dependent screening on the reaction phase diagram. *ACS Catal.* **2022**, *12* (11), 6781−6793.
(25) Suntivich, J.; May, K. J.; Gasteiger, H. A.; Goodenough, J. B.; Shao-Horn, Y. A perovskite oxide optimized for oxygen evolution catalysis from molecular orbital principles. *Science* **2011**, *334* (6061), 1383−1385.
(26) Suntivich, J.; Gasteiger, H. A.; Yabuuchi, N.; Nakanishi, H.; Goodenough, J. B.; Shao-Horn, Y. Design principles for oxygen-reduction activity on perovskite oxide catalysts for fuel cells and metal−air batteries. *Nat. Chem.* **2011**, *3* (7), 546−550.
(27) Peng, C.; Gao, L. Optical and photocatalytic properties of spinel $ZnCr_2O_4$ nanoparticles synthesized by a hydrothermal route. *J. Am. Ceram. Soc.* **2008**, *91* (7), 2388−2390.
(28) Chen, Y.-J; Li, B. Hydrothermal synthesis of $ZnMn_2O_4$ and its performance in lithium—ion battery. *Guangzhou Chem. Ind.* **2013**, *41* (2), 79−81.
(29) Sun, Y.; Liao, H.; Wang, J.; Chen, B.; Sun, S.; Ong, S. J. H.; Xi, S.; Diao, C.; Du, Y.; Wang, J.-O.; Breese, M. B. H.; Li, S.; Zhang, H.; Xu, Z. J. Covalency competition dominates the water oxidation structure−activity relationship on spinel oxides. *Nat. Catal.* **2020**, *3* (7), 554−563.

https://doi.org/10.1021/acs.nanolett.2c03598
Nano Lett. 2022, 22, 10003−10009